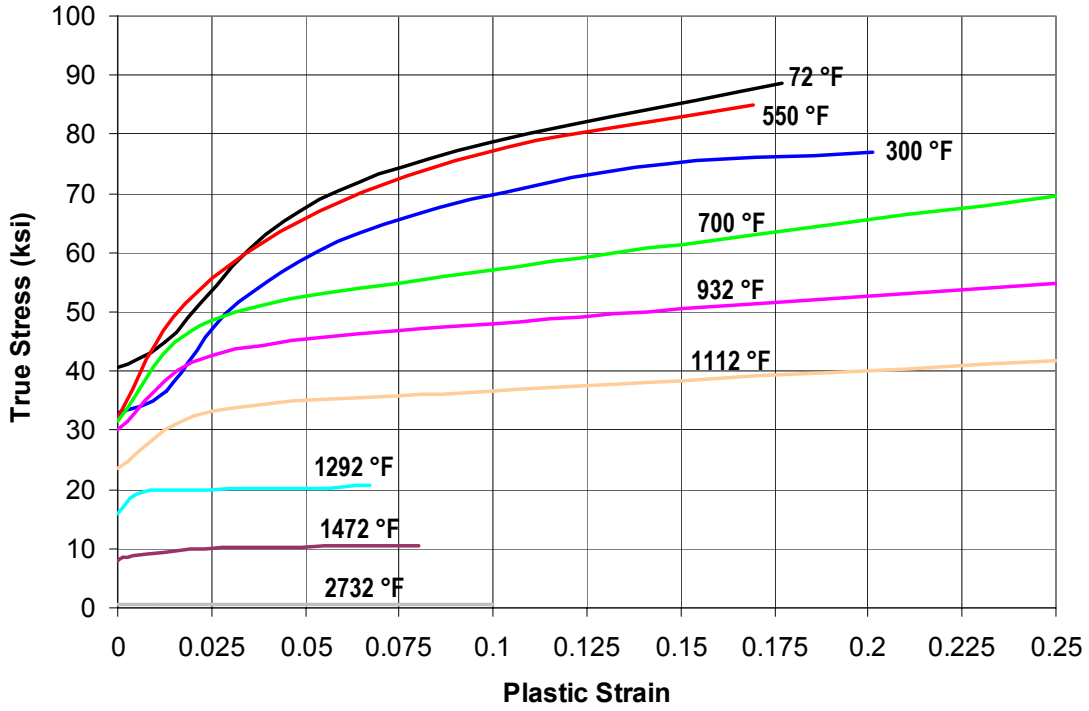

Figure G.7b Temperature dependent true stress-strain curves at A516 Grade 70

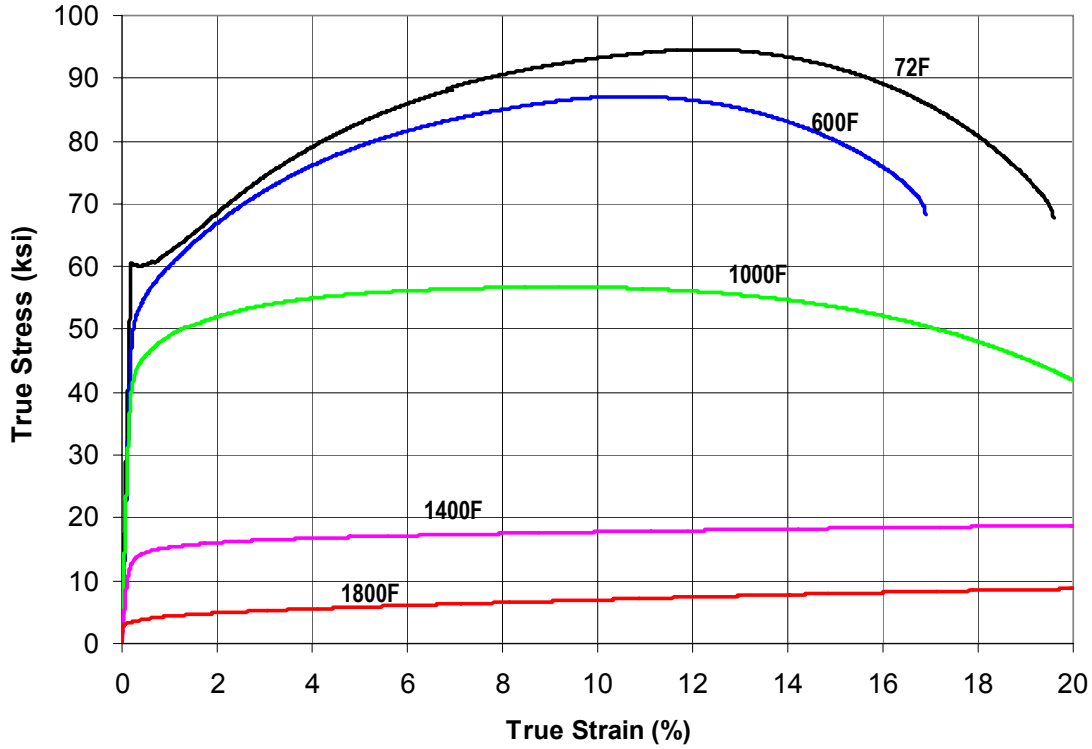

Figure G.7c Temperature dependent true stress-strain curves of A508 Class 3 tested by ORNL

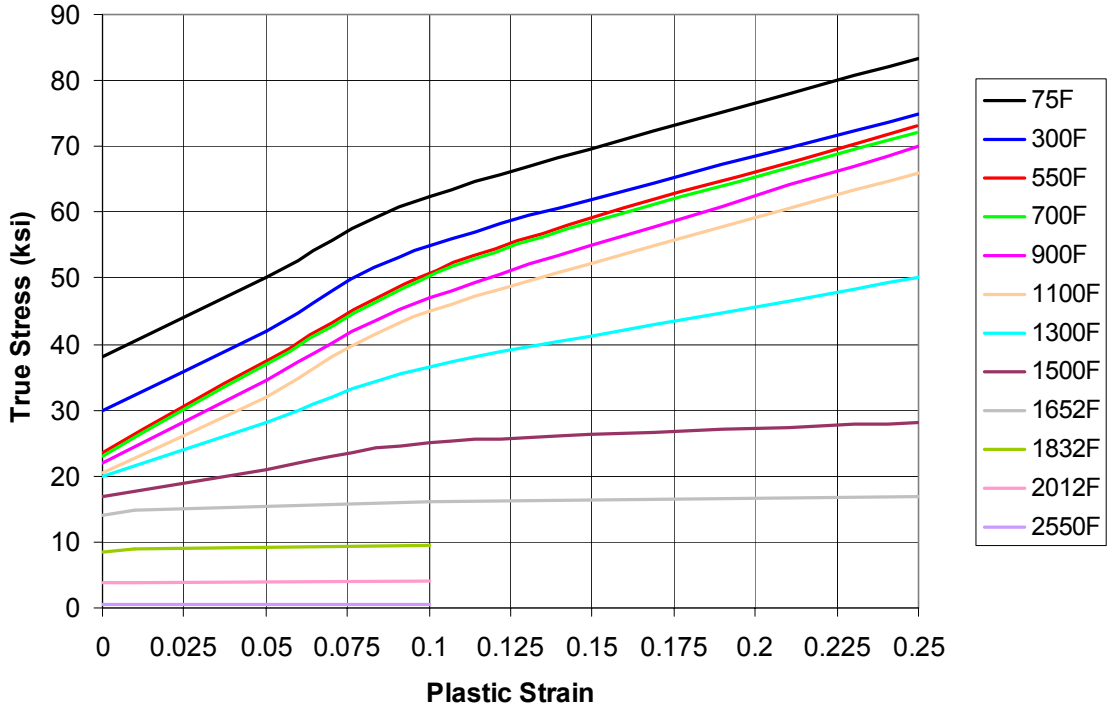

Figure G.7d Temperature dependent true stress-strain curves of Type 316 and Type 309

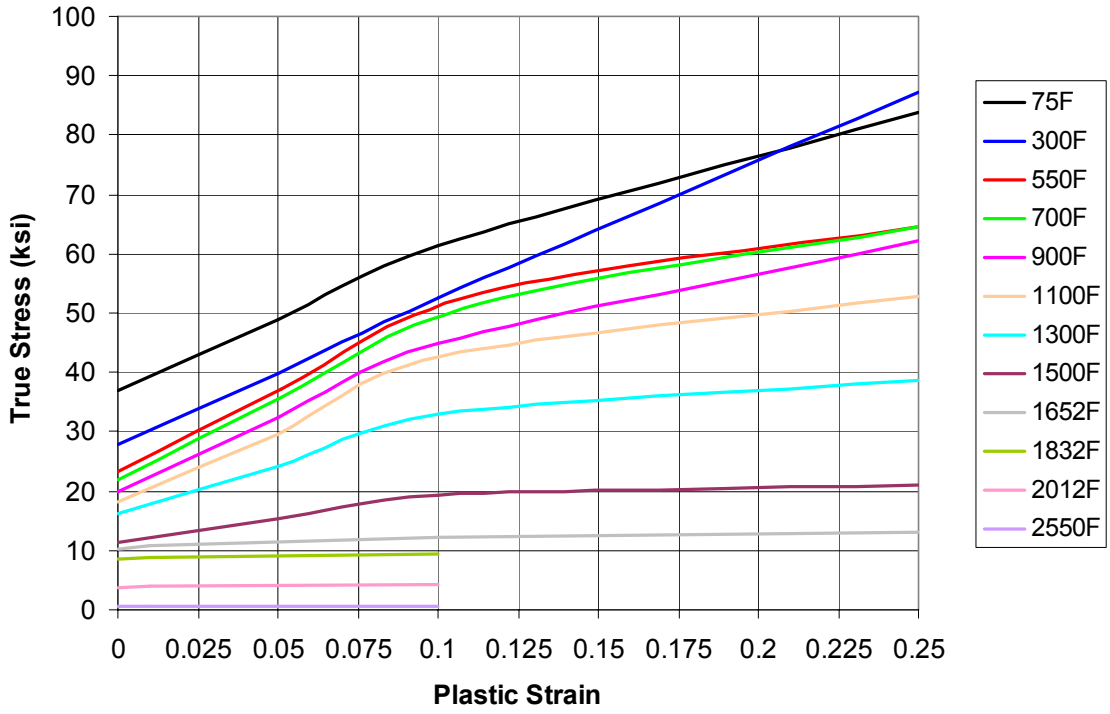

Figure G.7e Temperature dependent true stress-strain curves of Type 304

Table G.6 Temperature dependent creep constants for all the materials

$$\dot{\varepsilon}^{s} = \mathrm{A_s}\sigma^{n_s}$$

A_s	n_s	T
MATERIAL: A508 Class 2		
1.0000E-26	4.0000	70
2.2910E-12	6.0451	1000
3.2670E-07	4.8865	1200
3.2670E-07	4.8865	2500
Material: A516-70		
1.0000E-26	4.0000	70
2.5060E-13	6.3261	900
1.9920E-09	4.4071	1000
6.9010E-08	4.5039	1100
6.9010E-08	4.5039	2500
MATERIAL: S309, S304, S316		
1.0000E-26	4.0000	70
9.2650E-25	9.7800	887
4.6900E-24	9.9700	932
1.6410E-21	9.0600	977
3.9710E-19	8.2000	1022
2.7540E-18	8.2000	1067
1.7060E-17	8.2000	1112
1.1700E-16	8.1800	1157
7.2180E-16	8.1600	1202
3.4110E-14	7.4200	1247
1.3300E-12	6.7200	1292
2.0930E-11	6.2500	1337
3.2310E-10	5.7700	1382
MATERIAL: INCO182		
1.0000E-26	4.0000	70
1.0000E-26	4.0000	990
2.1478E-16	6.1709	1000
4.6025E-15	6.6426	1100
4.6025E-15	6.6426	2500

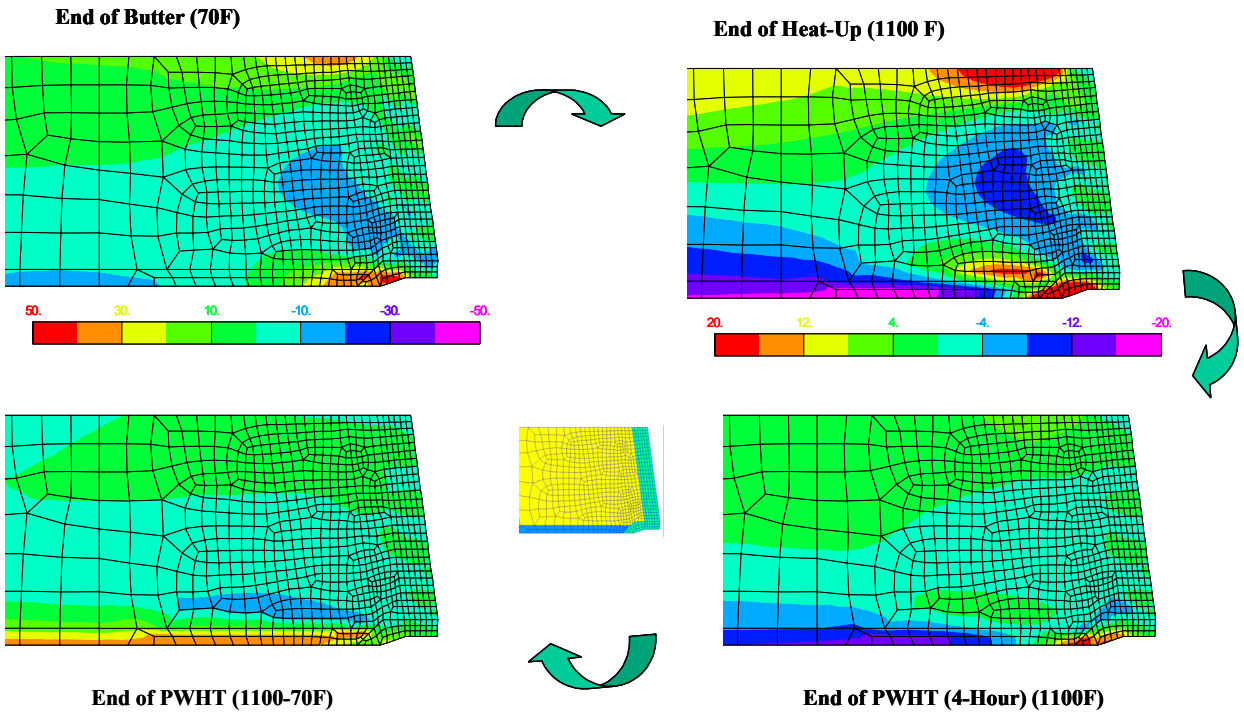

Figure G.8 Axial stresses during heat treat process

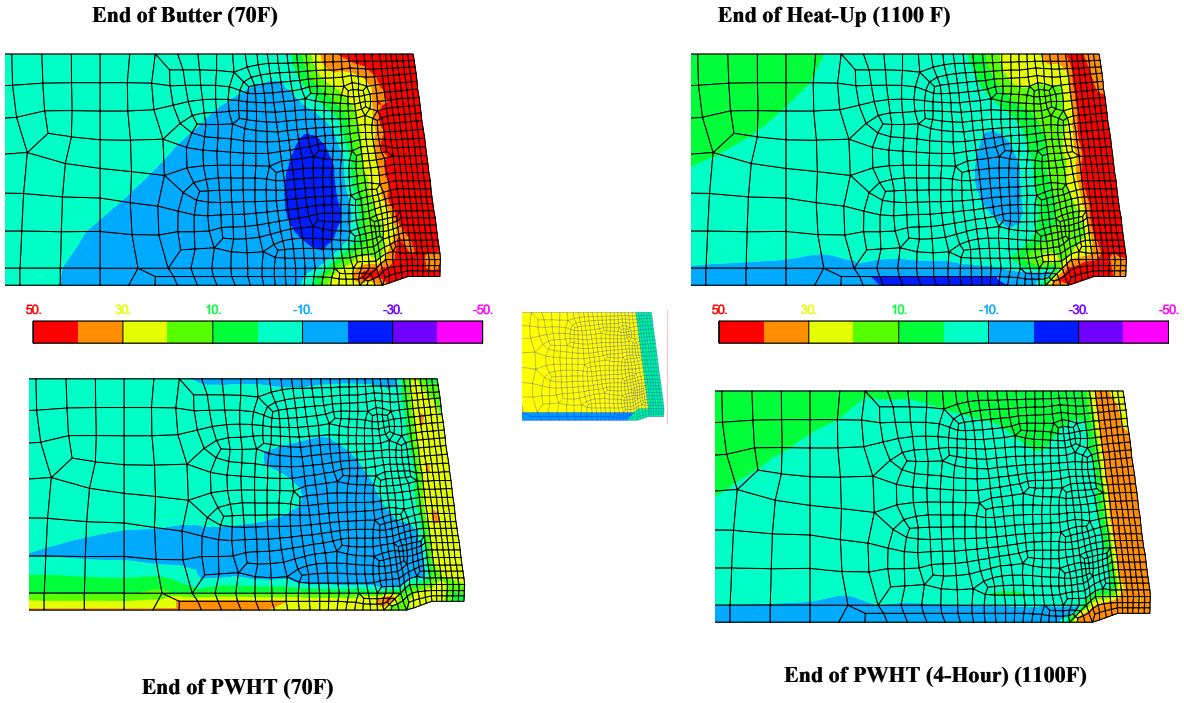

Figure G.9 Hoop stresses during heat treat process

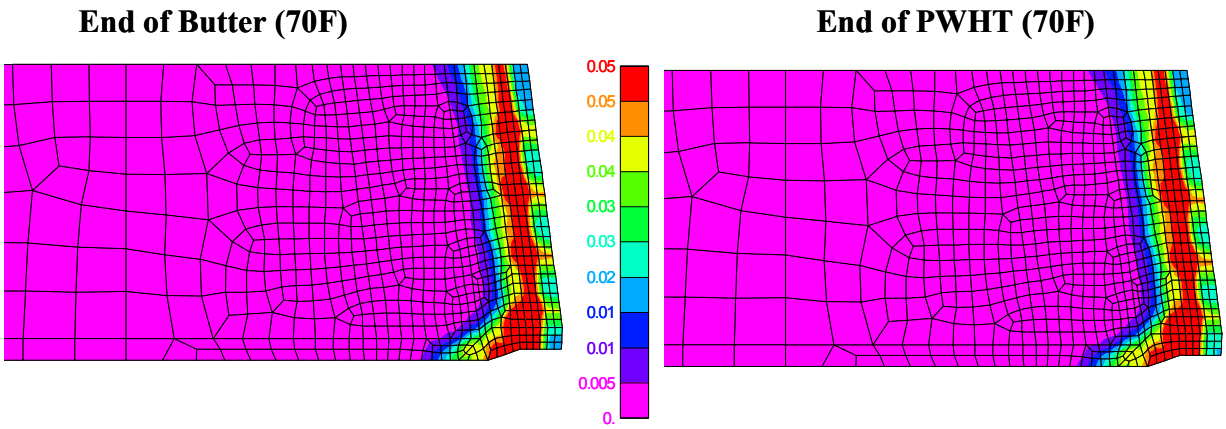

Figure G.10 Equivalent plastic strains

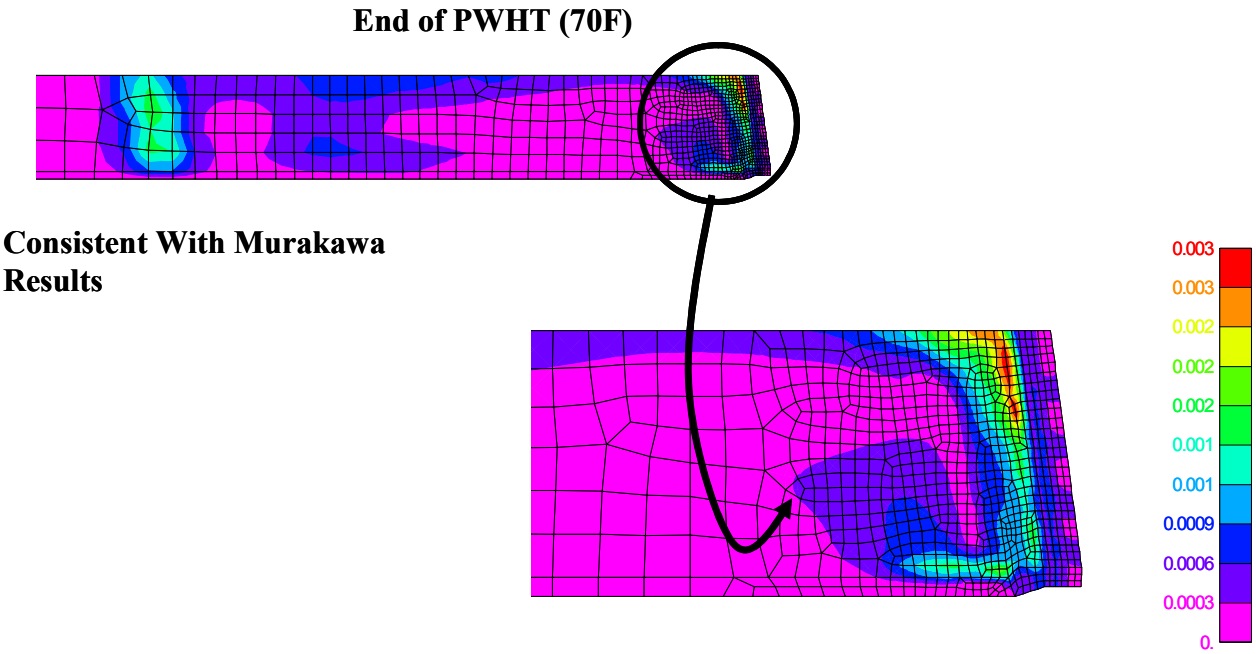

Figure G.11 Equivalent creep strains

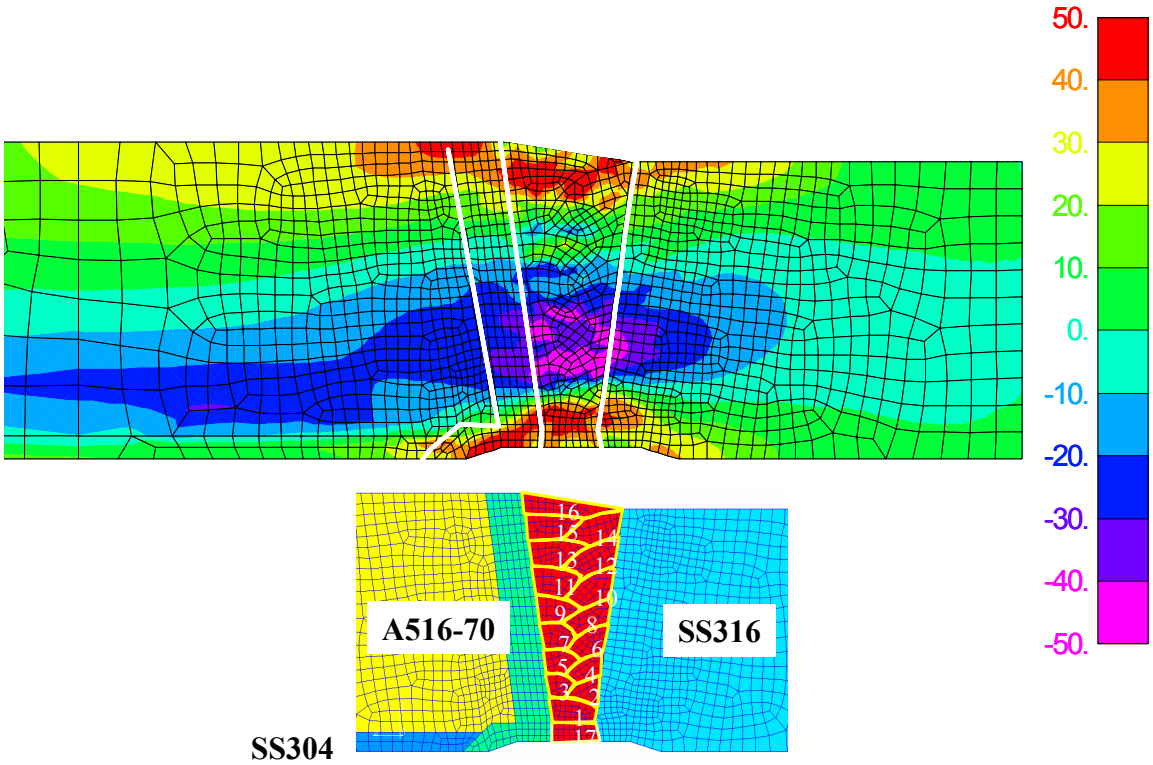

Figure G.12 Residual stresses final (axial) at room temperature 22C (70°F)

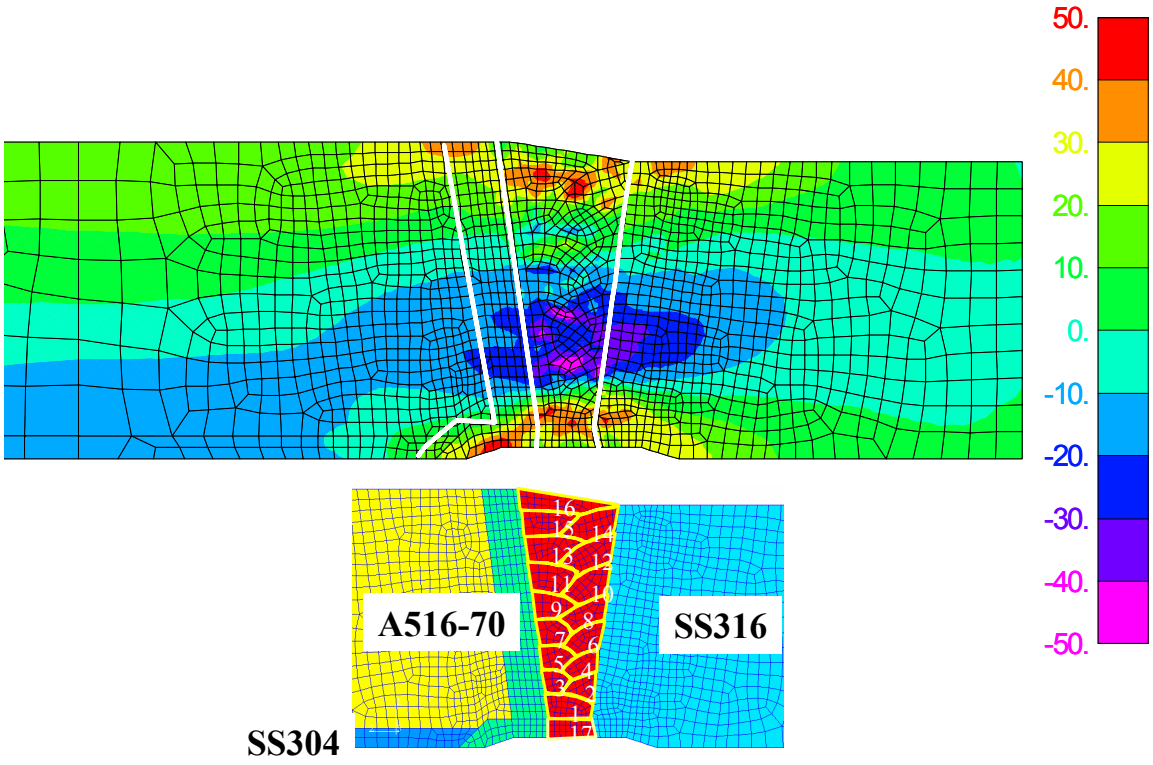

Figure G.13 Residual stresses final (axial) at operating temperature 291°C (556°F)

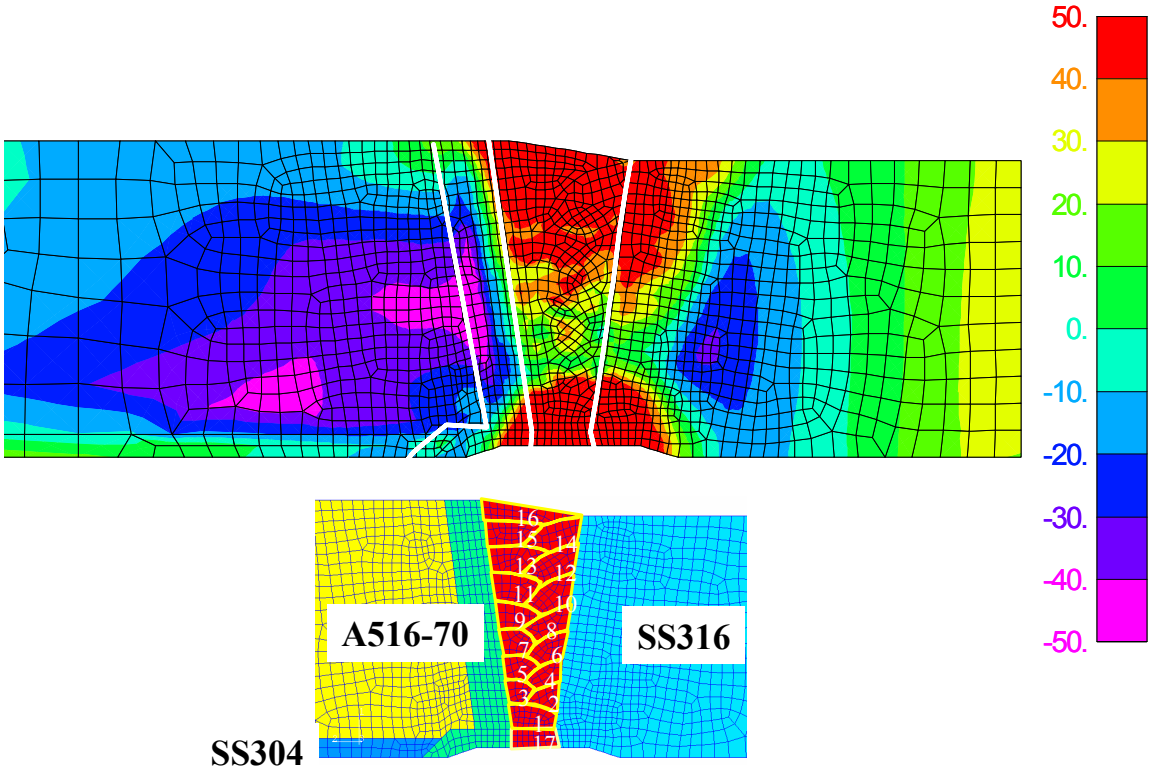

Figure G.14 Residual stresses final (hoop) at room temperature 22°C (70°F)

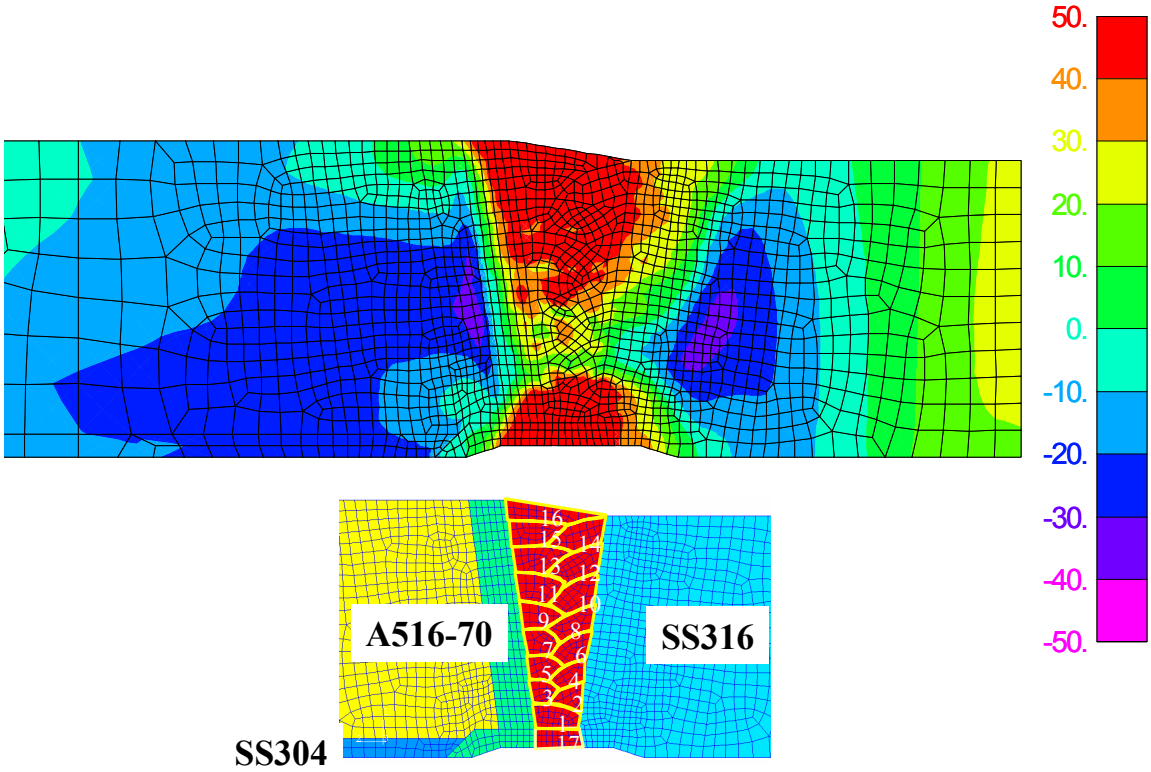

Figure G.15 Residual stresses final (hoop) at operating temperature 291°C (556°F)

through thickness stresses favor axial crack growth via stress corrosion cracking mechanisms if entirely driven by residual stresses.

Figures G.16 (a) and (b) show comparisons of axial weld residual stresses to measurements, while Figures G.16 (c) and (d) show the corresponding hoop stress comparisons. The measurements were made at Battelle at our West Jefferson, Ohio site, where the cold leg pipe has been stored since 1988. The 'chip removal' or trepanning technique of Reference G.6 (and many references sited therein) was used for the measurements. The trends for the axial residual stresses comparisons (Figure G.16 (a) and (b)) are similar, but the measurements are lower than the predictions. The hoop residual stresses (Figures G.16 (c) and (d)) measurements are quite low compared with predictions. Hoop residual stress measurements in bimetallic welds have not been reported in the literature as far as can be determined. However, from prior measurements and predictions of pipe (Refs. G.6 and G.9) for same material welded pipe and many reference sited therein), hoop residual stresses are nearly always tensile and approaching yield, especially in the regions of the weld for both thick and thin pipe. The measured stresses here (Figure G.16 (c) and (d)) are actually compressive in this region. This is considered unrealistic. Despite efforts to resolve this quandary, no errors in the measurement technique could be found.

Therefore, the main purpose of this analysis effort for the cold leg, to validate the VFT weld modeling procedure for bimetallic welds, was not successful. However, the results are useful and provide insight for the hot leg analysis discussed next. When the residual stress measurements were obtained, and the low values were measured, the weld modeling procedure was completely re-evaluated. The post weld heat treatment was then considered in the analysis process. The weld processes and procedures for both the cold leg and hot leg were carefully re-evaluated. The material properties used for the weld analysis were carefully evaluated. In fact, a separate test program was initiated at Oak Ridge National Laboratory (ORNL) to obtain better temperature dependent material properties for Inconel 182/82 weld metal and for A508 steel. It is important to recognize that the material properties of the weld material must be obtained on annealed weld samples because the weld modeling itself models the heating and cooling strain hardening explicitly. Hence, while the experimental residual stress measurements did not provide direct validation of the weld modeling, the insight that was obtained by considering all of the above processes was very important. Indeed, after all of these effects were considered, and re-analysis of the cold leg completed, the residual stresses predicted were lower than those originally predicted. However, they were still higher than the measurements. The fact that the hoop residual stresses measured at both the inside and outside surfaces are so low clearly indicates that the measurements were not accurate. Because the constraint in the weld direction (hoop direction) is high, as the weld bead cools, it shrinks and is constrained by the already cool material, producing high tensile residual stresses in all cases the present authors have seen in over twenty five years.

Measurement of residual stresses in bimetallic welds should be pursued in the future, perhaps using the new deep hole drilling procedures developed by Professor Smith of Bristol University (Ref. G.10). Regarding the trepanning method of measuring residual stresses, it has served very well in past studies at Battelle in the late 1970's and should be regarded as a viable method for measuring residual stresses. However, it requires a skilled and experienced technician to carefully remove the pyramid shaped chips from the pipe.

Figure G.17 illustrates equivalent plastic strains. Figure G.18 shows the corresponding axial, hoop, and shear plastic strains after welding. It is interesting to note that the axial plastic strains are compressive for the most part in the buttering region while the hoop plastic strains are tensile in the butter and weld. Moreover, from Figure G.18 (c), rather large values of shear strain develop in the region of the butter. While PWSCC growth is considered to be driven by tensile stress, or stress intensity factors, it may be useful to consider the role of tensile plastic strains in SCC growth in future studies.

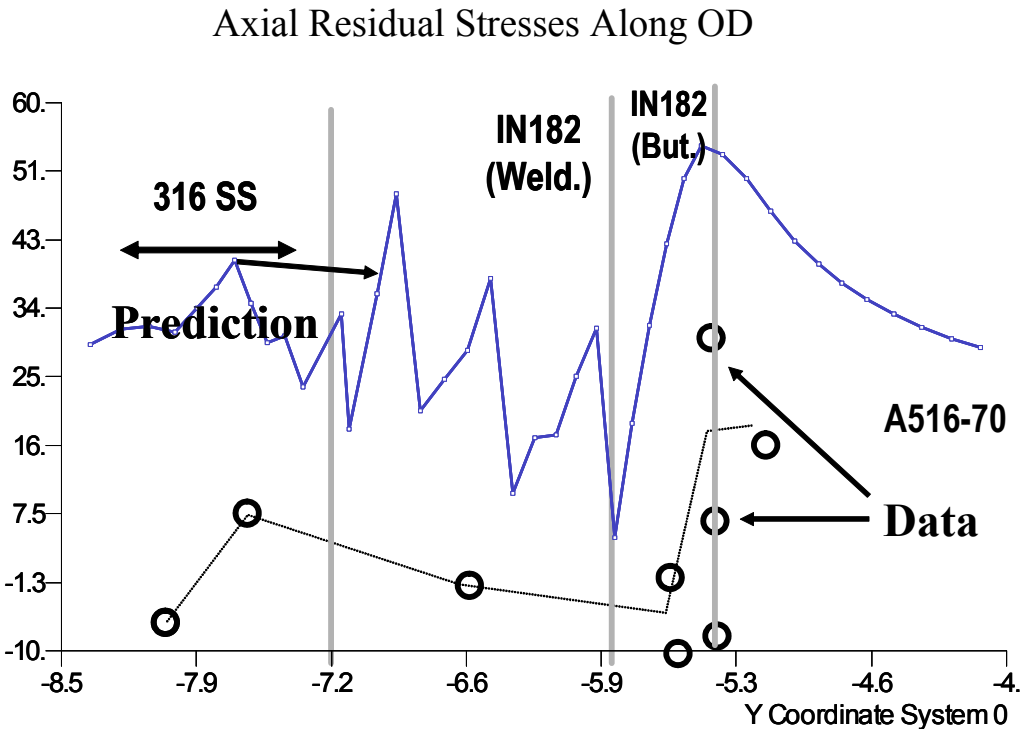

Figure G.16(a) Residual stresses final (axial) at operating temperature 291°C (556°F)

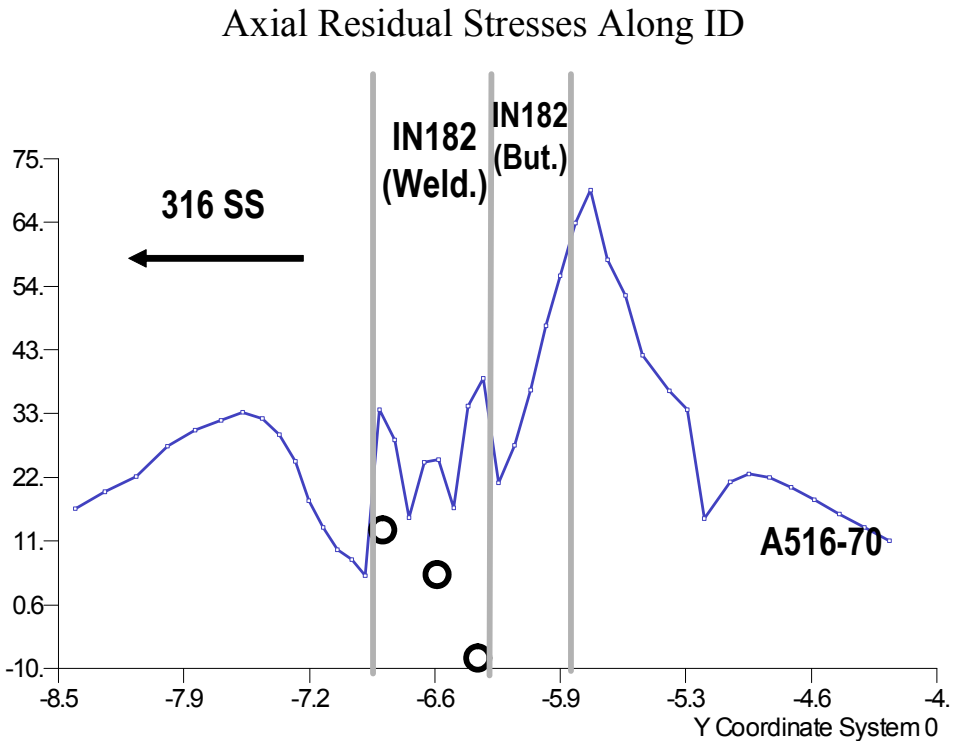

Figure G.16(b) Residual stresses final (axial) at operating temperature 291°C (556°F)

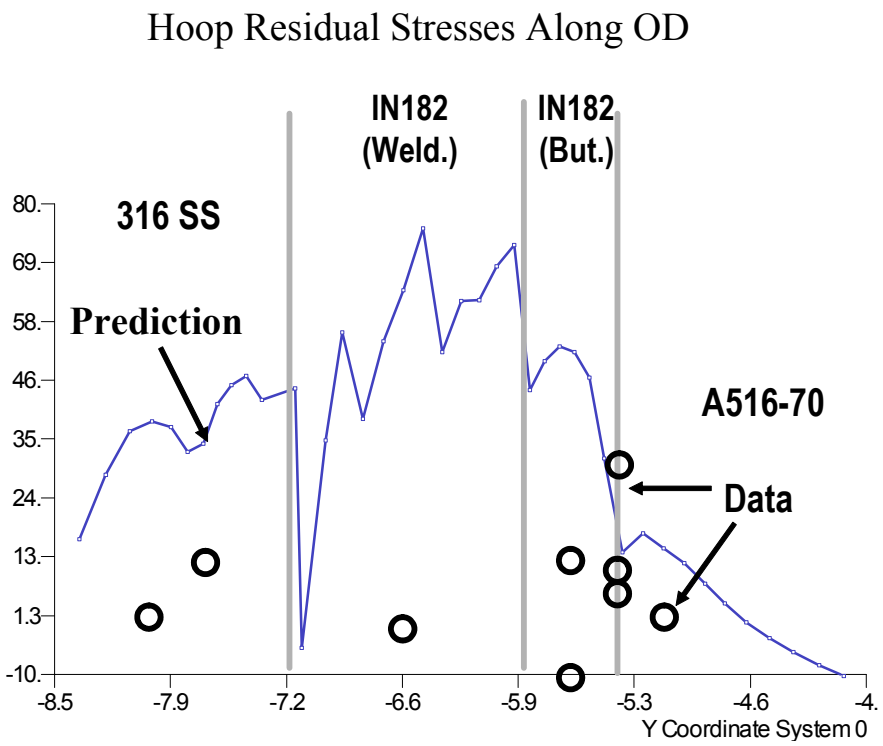

Figure G.16(c) Residual stresses final (hoop) at operating temperature 291°C (556°F)

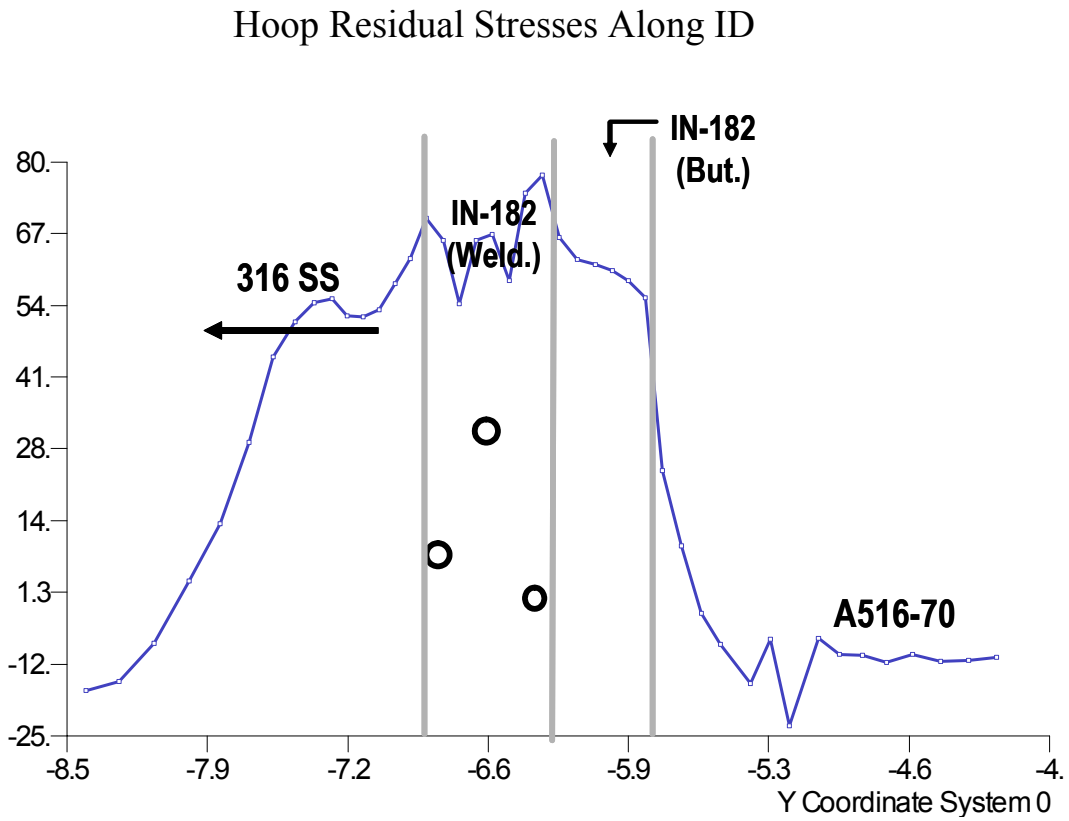

Figure G.16(d) Residual stresses final (hoop) at operating temperature291°C (556°F)

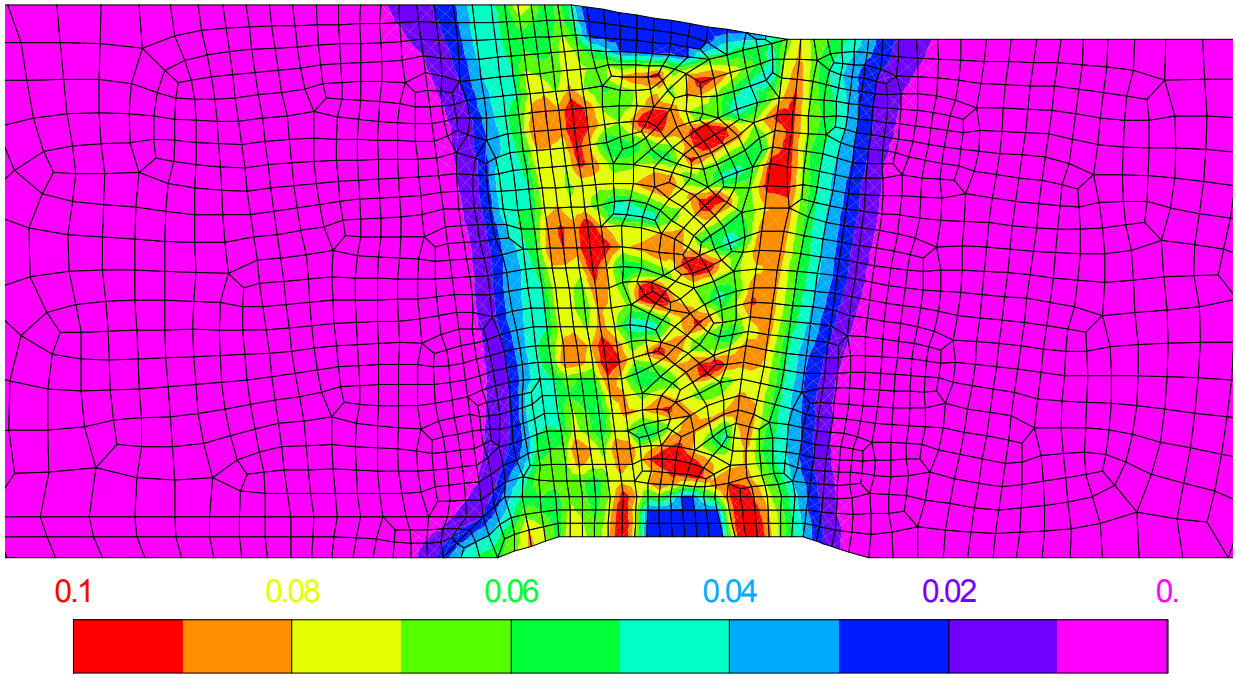

Figure G.17 Residual equivalent plastic strains in cold leg at room temperature

(a)

Axial

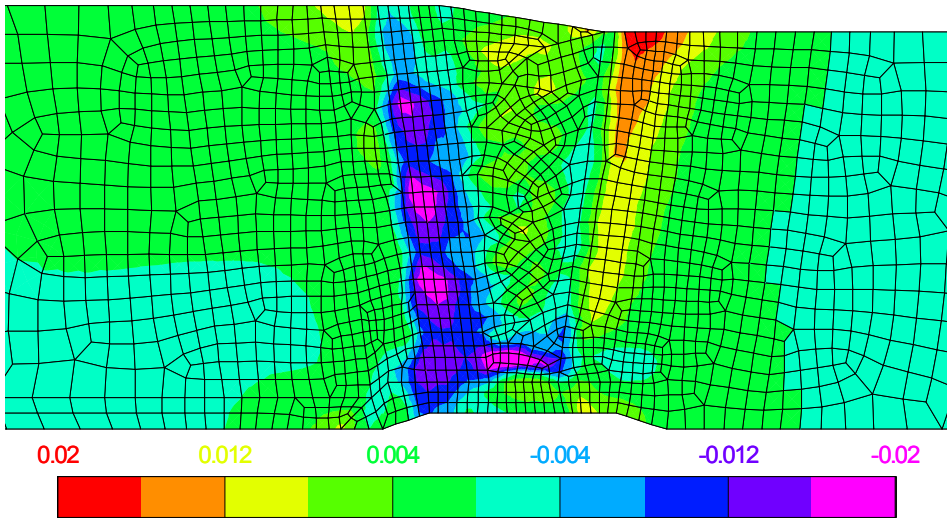

(b)

Hoop

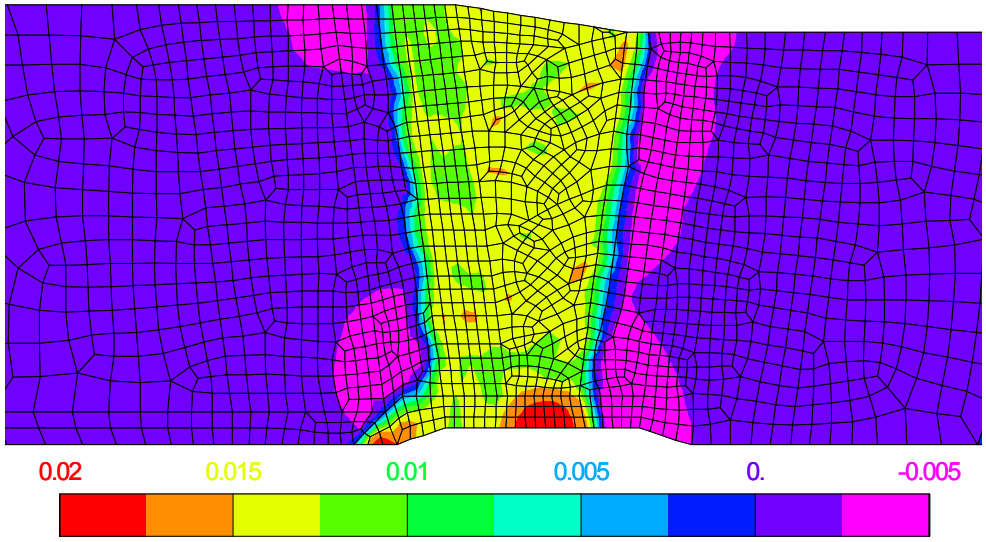

Figure G.18 Residual axial (a), hoop (b), and shear (c), plastic strains in cold leg at room temperature

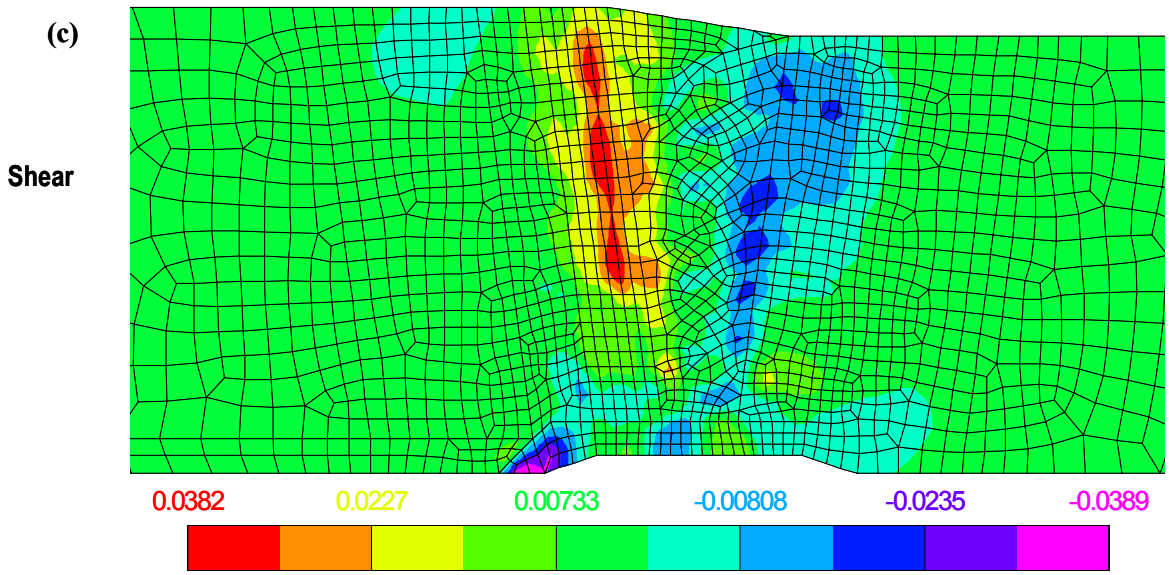

Figure G.18 Residual axial (a), hoop (b), and shear (c), plastic strains in cold leg at room temperature

G.6 RESULTS HOT LEG ANALYSIS

This section presents the axis-symmetric results for the hot leg analysis. The results of this analysis were used to calculate stress intensity factors so that PWSCC predictions could be made (Section G.7).

G.6.1 Hot Leg Computational Weld Model

The geometry of the hot leg bimetallic weld joint is illustrated in Figures G.19 and G.20. Note that the hot leg analysis for the V. C. Summer plant is similar to the cold leg analysis discussed in Section G.5 except that the geometry is different (smaller diameter and thickness), and the materials are different for the nozzle (compare with Figure G.3).

Please follow Figure G.21 for the description of the weld modeling process. The modeling sequence is quite complicated since the V. C. Summer hot leg in question had several repairs made to it. The sequence of the repairs was not entirely known, so two repair sequences were considered. Figure G.21 illustrates the welding sequence modeled. The nozzle was first pre-heated and a buttering layer deposited. The nozzle was then post weld heat treated (PWHT). As with the cold leg, the PWHT was modeled via creep analysis applied to the buttered weld residual stress state.

The buttered nozzle along with the stainless steel pipe was then pre-heated again and weld metal was deposited from the inside of the pipe to a depth of 18 mm (0.7 inch). After this amount of weld metal was deposited, the weld was rejected. In preparation for weld grind out (of the original 18 mm (0.7 inch) of weld metal), a weld bridge was deposited. The weld was then ground out from the pipe inside. There were then two weld sequences that were considered in the analysis since it was uncertain whether the weld repair was deposited from the bridge first on the outside of the pipe, followed by the inner weld or vice-versa. Both were modeled to examine the effect of the repair sequencing on the final residual stress state.

All of the processes listed in Figure G.21 were considered in the model. Figure G.22 further illustrates the modeling process pictorially. Figure G.22 (a) shows the original buttering model results. Figure G.22 (b) shows the PWHT modeling process. Figure G.22 (c) shows the completion of the weld prior to weld rejection, building of a weld bridge, and then

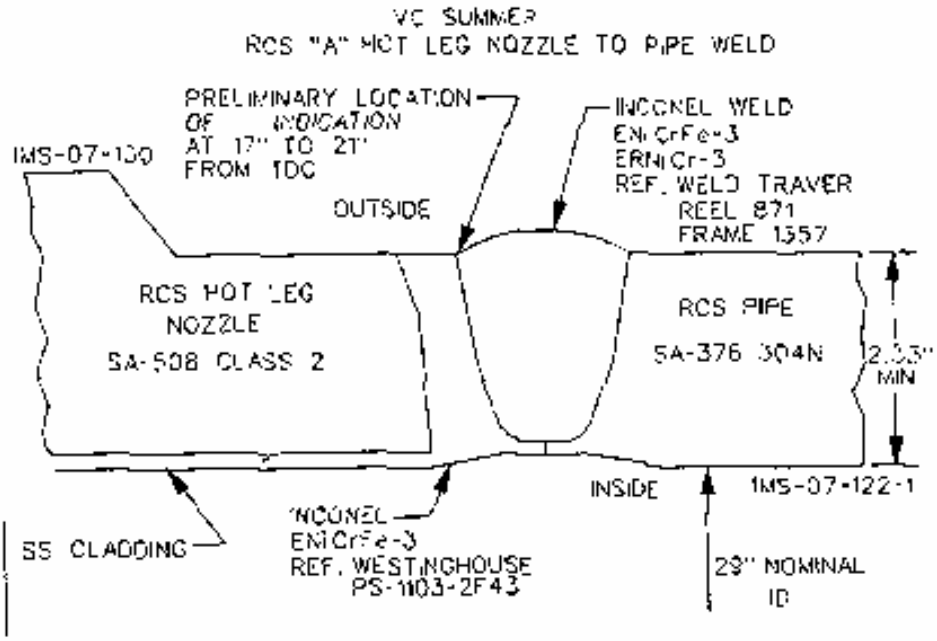

Figure G.19 Geometry of V.C. Summer bi-metallic weld joint

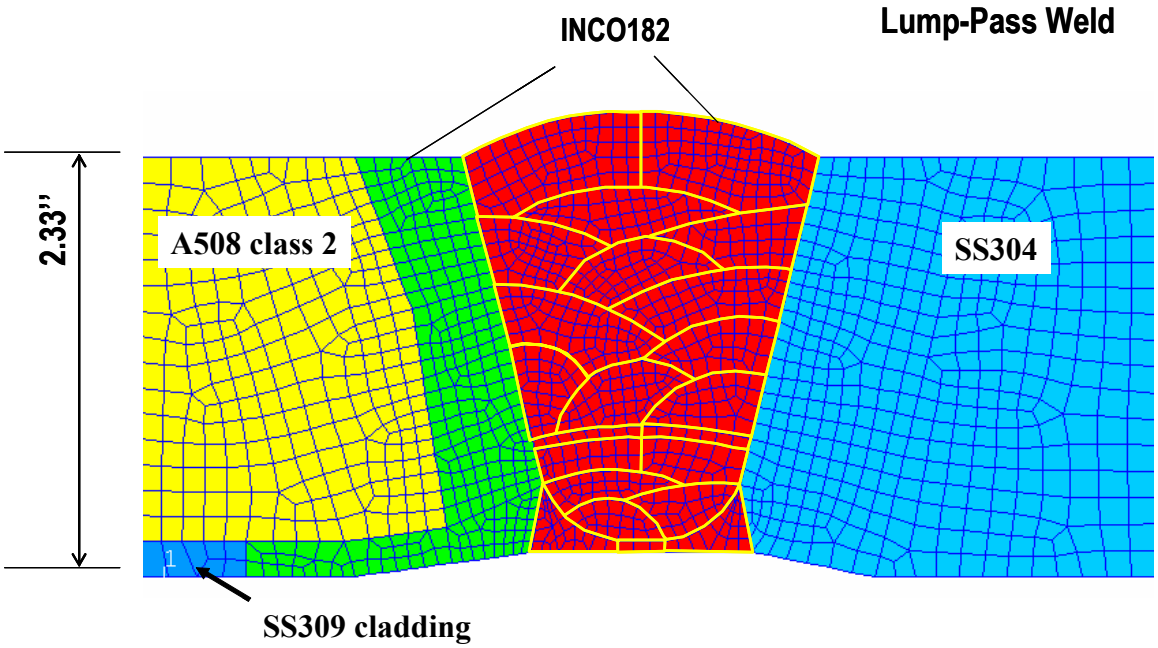

Figure G.20 Axis-symmetric model of V.C. Summer bimetallic weld joint

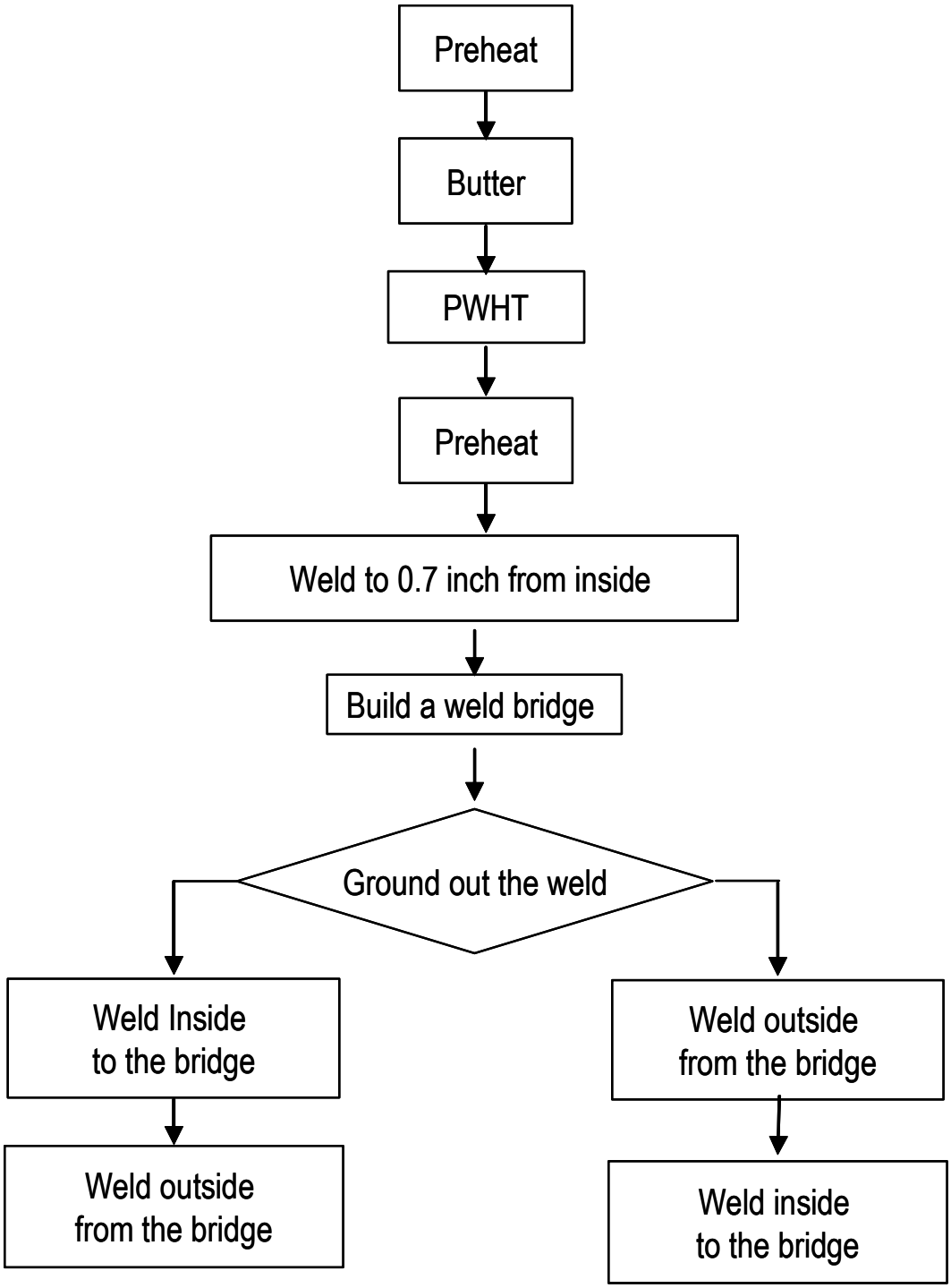

Figure G.21 Welding process simulated on hot leg

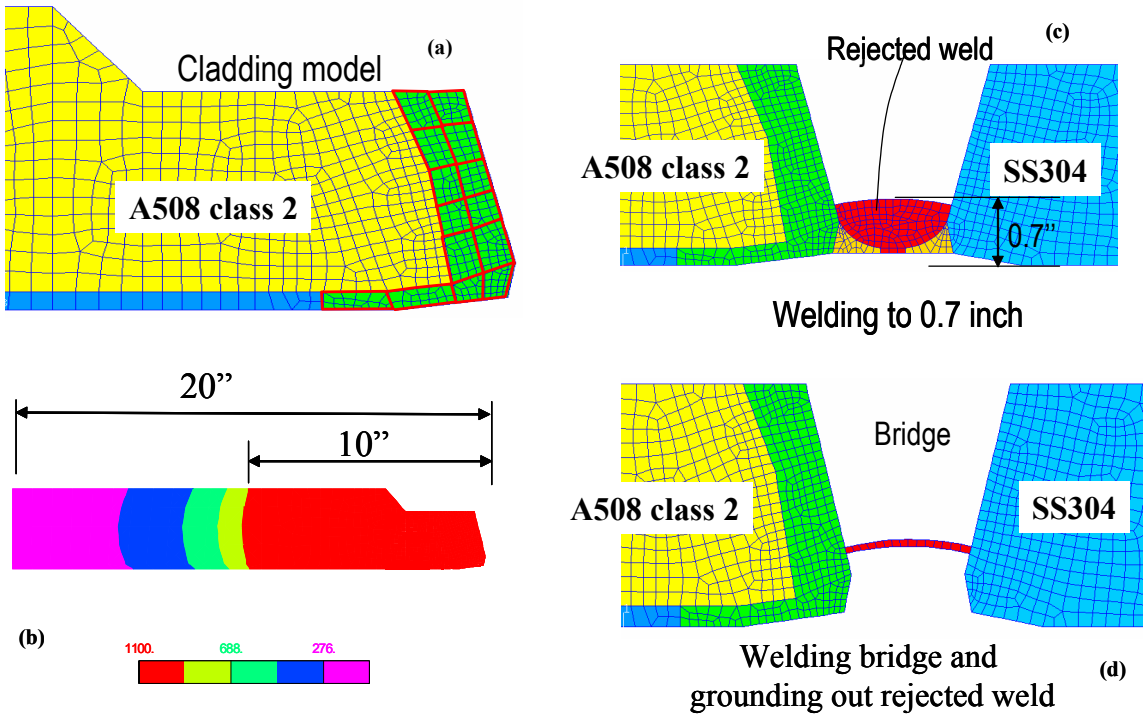

Figure G.22 Cladding (butter) and rejected weld model

grinding out the original weld so that only the bridge remains. Finally, the weld was either deposited from the inside surface first, then the outside surface, or vice-versa. Both were modeled since the precise repair weld deposition sequence was not known.

An important point regarding the analysis steps is in order at this point. Referring to Figures G.21 to G.23, grinding of weld material prior to deposition of the final weld passes was included in the modeling process. For instance, from Figures G.22 (c) to G.22 (d), material was ground out to make a bridge of weld metal prior to deposition of the weld repair layers. This grinding process simply consisted of removing material ‘computationally’. By this we mean that the material was removed mathematically by eliminating the stiffness of these elements and therefore redistributing the residual stresses. The actual grinding process, whereby a rigid (or nearly rigid) sharp tool impacted the weld region and material was ‘chipped away’ was not considered. This is a complex modeling problem, but it can be done. However, the main effect of the grinding is to redistribute the residual stress state in the pipe as material is removed and the precise modeling of the chipping process is not necessary.

There is another source of grinding that occurs after the entire weld repair is completed. Reference G.12 provides summary of the metallurgical investigation of the cracking in the V. C. Summer plant. As discussed on page 9 of Reference G.12, ‘The surface appeared highly irregular with evidence of significant surface grinding and machining distress marks’. Photographs and micrographs clearly show small ‘scratch marks’ along the inner pipe surface at the weld location (Figures 10 and 19 from Reference G.12). This grinding was presumably performed in order to remove the weld repair ‘bulging’ at the pipe inside surface in order to permit more uniform flow through the pipe. The grinding will redistribute residual stresses (as discussed above regarding the grinding before weld repair). However, because the material ground out is a small volume, it is not included in the analysis (i.e., the final geometry, already ground, is modeled).

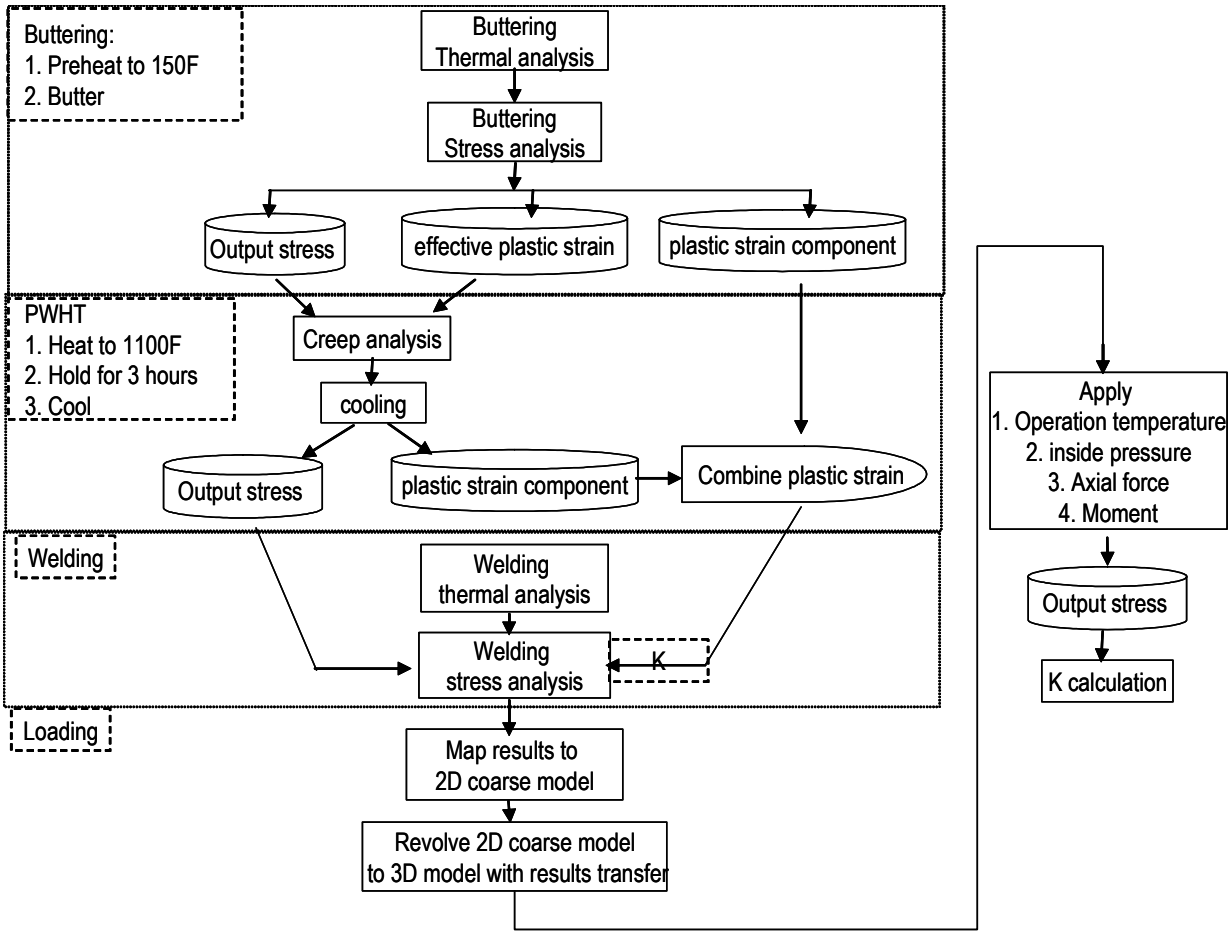

Figure G.23 Finite element analysis process flow

In essence, if additional material was added to the inside surface weld, and then removed, the final residual stress state should be very similar to that from ignoring it except for very localized grinding stresses. The very local residual stresses from the grinding process are ignored in this case. Typically, additional residual stresses from grinding are considered to be important for only a very short depth into the thickness of the pipe. Certainly, after the crack grows a very short distance into the pipe thickness, these local residual stresses are eliminated and the weld induced residual stresses dominate for most of the PWSCC growth life.

However, the geometric effects of the scratches are expected to be very important. These scratches should be considered as crack initiation sites for PWSCC, fatigue, or any possible cracking mode. Such grinding, which produces scratches, may serve as PWSCC initiation sites and should be avoided. It may be a useful exercise to include the actual modeling of grinding in such a model as an additional step in order to further prove this hypothesis. Moreover, since grinding is common practice, and is apparently not specifically considered by the code bodies, such a series of 'grinding' model studies may be of use in setting standards in future construction and aging repair.

G.6.2 Hot Leg Computational Weld Model – Buttering and PWHT Results

Figure G.23 illustrates the entire analysis procedure for the hot leg. As seen, after the weld modeling is completed, results were mapped to a coarser two-dimensional model. The coarser two-dimensional model was then revolved to a three-dimensional model in preparation of the three dimensional PWSCC crack growth analysis. Service loads were then applied and